Report No. 127

February, 1960

THE COLLEGE OF AERONAUTICS

CRANFIELD

Ablation Studies of Low Melting Point Bodies in a Pre-heated Supersonic Air Stream

- by -

J. W. Cleaver*, B.A., D.C.Ae.,

and

F. Thomson*, B.Sc., D.C.Ae.

SUMMARY

This report is an investigation into the melting of axi-symmetric and two-dimensional bodies at a Mach No. of $M_\infty = 1.78$ and stagnation temperatures up to 550°K. In this temperature range, the most suitable material for the models was found to be an eutectic tin-lead alloy with a melting point of 456°K.

For the cone and hemisphere-cone models two distinct modes of melting were observed. In cases where the estimated equilibrium surface temperature $(T_w)_o$ was approximately equal to the material melting temperature T_m, melting occurred only at the stagnation point of the model and was such that a flat surface normal to the gas stream always resulted. If the average rate of heat transfer at the air-liquid interface be defined as $\dot{q}_i = L_m \rho_m \dot{x}$, where L_m is the latent heat of fusion, ρ_m is the density of the material and $\dot{x}$ is the rate of recession of the flat surface, it is found that $\dot{q}_i$ decreases with increase of the radius of the flat nose. A very approximate theory is found to show some agreement with the experimental rates of heat transfer. When $(T_w)_o$ was considerably greater than T_m the flat surface was no longer preserved and the resulting steady ablating shape was paraboloidal in nature. When this occurred $\dot{x}$ was usually constant. This allowed some average steady state heat transfer rates to be evaluated and compared with theory.

Preliminary tests were also made with a two-dimensional wedge model.

---

* Based on a thesis submitted in partial fulfilment of the requirements for the Diploma of the College of Aeronautics.

LIST OF CONTENTS

		Page
	Summary	
	List of Symbols	
1.	Introduction	1
2.	Test Equipment and Calibration of the Instruments	2
	2.1. Description of the apparatus	2
	2.2. Calibration of the Equipment	3
3.	Experimental Procedure	4
	3.1. Operation of the Tunnel	4
	3.2. The Melting of Axi-Symmetric Bodies	4
	3.3. Melting of Two Dimensional Bodies	5
4.	Discussion	5
	4.1. The Wind Tunnel	5
	4.2. Choice of the Model Material	6
	4.3. Model Surface Temperatures	7
	4.4. The Design of the Shrouds	7
	4.5. The Ablation of Axi-Symmetric Bodies	7
	4.6. The Two Dimensional Model	9
5.	Conclusions	10
6.	Acknowledgements	10
7.	References	11
	Appendix A - Simplified Analysis of Melting for which $(T_w)_o \simeq T_m$	12
	Appendix B - Ablation of cones and hemispheres for which $(T_w)_o \simeq T_m$	14
	Tables	
	Figures 1 - 20	

2.1.2. Pressure measurements

The stagnation pressure of the tunnel was measured with a static probe located in the settling chamber. At the working section the static pressure was obtained by a tapping in the floor of the tunnel and the total head traverses were made with a pitot tube.

2.1.3. The temperature probes

The probe used for measuring temperature is shown in Fig. 5 and consists of chromel-constantan thermocouple shielded by two concentric tubes of duralumin. The recovery factor of this type of probe is about 0.99 over the Mach number range encountered in this report. This type of probe was used for measuring the total temperature in the working section and the settling chamber. The temperatures were recorded on a standard Foster instrument

2.1.4. The traversing rig

This has been described in Ref. 6 and was used for the pressure and temperature measurements which were made in the working section.

2.1.5. The wedge models

The wedge used to simulate a two dimensional mode of melting is shown in Fig. 1. In order that temperature variations within the material could be investigated the model was constructed so that only the upper half of the wedge melted. The upper half was made of a low melting point material and the remainder of the model manufactured from a material with a melting point much higher than the temperatures expected to be realised in the tunnel. Previous investigations (Ref. 7) indicated that if the thermal properties were ill chosen then the heat transfer from the support to the ablating material could considerably influence the melting process. Thus, the base of the model which held the insert of ablating material was made of brass. Experiment confirmed that the thermal properties of this material were comparable to those of the insert thus resulting in a thermally homogeneous.

Before tests were made on the above model it was thought desirable to find out if a temperature variation existed over the surface of the model. To do this a steel wedge, illustrated in Fig. 2, was made containing a copper insert in the surface, in which seven thermocouples were embedded. Each thermocouple consisted of one constantan wire, with the copper insert acting as the other element of the thermocouple. The constantin leads were insulated with ceramic tubing from the surrounding copper, contact being made only at the surface of the copper (Fig. 2). This minimised the possibility of short circuiting the thermocouple.

2.1.6. The A.R.L. 12 Channel Recorder

This instrument enabled 12 input voltages to be recorded simultaneously. It consists of 12 A.R.L. Midget Galvanometers with each channel fully insulated. The inputs are measured by the deflection of the mirror galvanometer, which are recorded by reflecting a light source (a loop filament lamp) from the mirros on to the sensitised paper. The trace width obtained is 0.005" and therefore with a deflection of 0.5", an accuracy in reading of 1% may be achieved.

A reference trace is provided by a static reflecting mirror, and lateral adjustment is available for siting the trace at any convenient spot across the sensitised paper. Light from each galvanometer is momentarily interrupted and by noting the sequence of interruptions the traces may be identified along the entire length of the paper, although they may run closely or cross.

The scale deflection is regulated by the insertion of a series resistance in the circuit, whilst a shunt resistance of appropriate value will give any desired degree of damping.

2.1.7. The Axi-Symmetric Heat Transfer Models

These models were cone-hemisphere-cylinder shaped bodies as shown in Fig. 10a and were constructed of tin or tin-lead alloys. The included cone angle varied from 15° - 40° and the nose radius varied from zero to 5/16" radius.

To investigate the effect of high stagnation temperature on the mode of ablation, it has been necessary to design a shroud which would fit over the model and reduce the heat transfer to the model long enough for a predetermined stagnation temperature to be reached.

The shroud consisted of a hollow wooden cone split in two; the pieces of which were held together by copper wire soldered with tin and by a nose piece made of tin (Fig. 3). When the tin melted the shroud was blown off leaving the model exposed to a stream temperature approximately equal to the melting temperature of the tin. To reduce heat transfer further, asbestos wool was packed between the shroud and the model. The base of the model was protected by an asbestos washer.

2.2. Calibration of the Equipment

2.2.1. Wind tunnel

Total pressure traverses were made throughout the area of the working section. With the throat pads in position it was found that uniform flow only existed in the middle of the working section (Fig. 6) and the average Mach number was $M_{\infty} = 1.78$. Without the throat pads however the uniform flow was maintained up to the tunnel walls and the Mach number was $M_{\infty} = 1.65$.

The decrease in the Mach number obtained near the walls when the throat pads were inserted was due to reflected shock waves associated with the non-uniform flow in the nozzle.

The temperature traverses indicated that throughout the working region a fairly uniform temperature existed (Fig. 7).

2.2.2. Calibration of the Thermocouples

The total temperature probes for measuring the gas temperatures, and the thermocouples in the wedge model, were calibrated complete with their ancillary equipment against a master thermocouple. The wedge model and the tunnel thermocouples were placed with the master thermocouple inside an electric oven and the readings obtained from the A.R.L. recorder and theFoster instrument were compared with the temperature indicated by the master thermocouple.

In order to ensure that a uniform temperature existed throughout the oven it was allowed to settle for at least fifteen minutes before each reading was taken. This allowed all thermocouples to reach a common temperature.

3. Experimental Procedure

3.1. Operation of the Tunnel

The general procedure for operating the tunnel, together with the safety precautions which should be observed, has been fully described in Ref. 6. It should be noted that in these experiments a prescribed temperature could not be obtained instantaneously. The time lag for the stagnation temperature to reach a required steady value was of the order of several minutes. However, once the required stagnation temperature was obtained, it could be maintained to within $\pm 3^{\circ}C$, or better.

3.2. The Melting of Axi-Symmetric Bodies

3.2.1. Ablation tests for $(T_w)_o \approx T_m$

A hemisphere-cone model of known metal and geometry was attached to the sting and the gas temperature slowly increased until the stagnation temperature (T_s) was such that the wall temperature $(T_w)_o$, of the model was approximately equal to the melting temperature T_m, of the material. This stagnation temperature was then maintained during ablation. The mode of melting was recorded by the Bolex 35 mm camera.

3.2.2. Ablation Tests for $(T_w)_o > T_m$

In this series of tests the bodies melted were identical to those used in the previous section. The test procedure was modified to give $(T_w)_o > T_m$ where $(T_w)_o$ is the equilibrium wall temperature for an unablated body that is, when $(T_w)_o$ was just below the melting temperature the fuel pressure was rapidly increased and then continuously adjusted to maintain a fairly constant stagnation temperature. This, however, limited $(T_w)_o$ because of the time lag mentioned above.

3.3. Melting of Two Dimensional Bodies

The experimental procedure was similar to that described in 3.2.1.

3.4. Investigation of Wall Temperatures

The non-melting model described in section (2.1.5.), was used to investigate the relation between stagnation temperature and surface temperature. In these tests the stagnation temperature was allowed to attain a steady value before surface temperatures on the model were obtained using the A.R.L. records. This was repeated for stagnation temperatures in the range $430^{\circ}K < T_s < 560^{\circ}K$.

Tests were also made using temperature indicating thermindex paints and tempilaq. These were coated on the model and the stagnation temperature at which colour changes occurred, was noted.

4. Discussion

In Ref. 7 the preliminary investigations indicated that the mode of ablation was influenced by the model material and the flow characteristics of the wind tunnel. These two factors were therefore examined before the work of Ref. 7 was pursued further.

4.1. The Wind Tunnel

The tunnel flow has been described in section (2.2.1) and attention was drawn to the existence of reflected shocks originating at the throat and causing certain non-uniformities in the flow in the working section. Since the axi-symmetric models were within the uniform region their mode of melting was unaffected by the presence of these non-uniformities. In the two dimensional tests however, the wedge extended across the full width of the working section and therefore the possible influence of these non-uniformities on the melting process must be allowed for.

Reference 6 discusses the flow separation in the diffuser following the working section, which induces severe vibrations in the tunnel. The flow characteristics appeared to be unnaffected by these vibrations, although some of the scatter obtained in the heat transfer results may be caused by the vibrations resulting in some instability of the liquid layer.

4.2. Choice of the Model Material

Bogdonoff (Ref. 1), briefly describes some tests in which ice and carbon dioxide models were ablated in the Princeton Hypersonic Tunnel. With the tunnel described in this report practical difficulties prevented tests being made with these materials, thus for ease of handling, a low melting point metal was used.

As the tunnel could be operated safely only up to a stagnation temperature of 550°K, tin, with a melting point of 505°K and its alloys were considered to be suitable. These materials were used in Ref. 7 and the filmed records indicated that the melting was a discontinuous process, with lumps of semi-molten material being torn away from the model instead of being ablated continuously. Naturally in such tests no reliable melting rates could be obtained.

Metallurgical analysis of the materials used in Ref. 7 showed that they were, (a) pure tin (chempur 99.992 %Sn), and (b) Plumbers solder (non-eutectic lead-tin alloy, 70% Pb., 30% Sn.). A series of ablation tests were performed on cone models using these materials and also the following, (c) Tin - No. 2 industrial pure (99.75 % Sn), (d) Tin-lead-eutectic alloy (37% Pb, 63% Sn), and (e) Tin-lead non eutectic alloy (60% Pb, 40% Sn).

For the models made of metals (c), (e) it was found that initially a slight melting of the cone tip occurred, but thereafter the model disintegrated. Similar effects were experienced with metal (b) except that the break up of the model was not so violent and the process was extended over a longer period. Photomicrographs for metal (c) (Fig. 19a) revealed that the impurities existing in the grain boundaries were in sufficient quantity for local melting to occur. This would result in local loss in strength and the aerodynamic forces on the body would be sufficient to cause the observed disintegration. For the two non-eutectic metals (b,e) no unique melting point exists and thus local melting would once again result in local losses in strength.

The chempur tin models did not disintegrate in this manner, but exhibited an unusual model of melting. Small irregular angular blocks (Fig. 16) of metal broke off from the nose of the model and this characteristic persisted until the whole model had ablated. The photo-micrograph (Fig. 19b) is typical of pure tin and yields no explanation for this phenomenon. Reference 4 has found however that at elevated temperatures, especially near the melting point the strength of tin is drastically reduced and so under the action of the aerodynamic forces the tin is slowly torn apart before it has reached its melting point.

The eutectic alloy displayed none of these characteristics and was the only one to melt in a continuous manner yet maintain sufficient strength at the higher temperatures to withstand the aerodynamic forces. The photo-micrographs (Fig. 19a) shows the homogeneity of the alloy. Thus the eutectic tin-lead alloy was chosen as the most suitable material for further investigation of ablating processes at these low stagnation temperatures.

4.3. Model Surface Temperatures

The results of the tests mentioned in section (3.4), on the wedge models to find the relationship between surface temperature and the stagnation temperature is shown in Fig. 8 and a linear relationship was obtained between T_s and T_w. The exhaust gases from the pre-heater will pollute the air stream and thus reduce the value of the ratio of specific heats γ. An approximate analysis suggested that γ lies within the range $1.30 < \gamma < 1.35$. The latter approximation to γ was used in determining the Mach numbers. It was found that with a recovery factor of 0.88 theoretical prediction of T_w is satisfactory for the cases $M_\infty = 1.78$ and $M_\infty = 1.65$, see Fig. 8. Further, thermindex tests on the axisymmetric bodies showed results not inconsistent with the wedge model. Since the surface temperature of the melting bodies could not be measured, the above relationship between the stagnation and surface temperatures was used to estimate the gas-liquid interface temperature.

4.4. The Design of the Shrouds

As described in section (3.2.2) to obtain $(T_w)_o$ much greater than T_m a means of reducing heat transfer into the model was required whilst T_s was raised to the appropriate value. Initially, a hollow wooden cone split into two halves and placed over the model and held together by tin soldered wire was used. This, however did not provide sufficient protection, but by fitting a tin nose cone to the wooden shroud and packing it with asbestos the required reduction in heat transfer was obtained. The final design adopted is shown in Fig. 3 and is described in section (2.1.7).

4.5. The Ablation of Axi-Symmetric Bodies

Little work on experimental liquid-ablation has been published. However results similar to those obtained in this report have been reported by Bogdonoff (Ref. 1) who subjected ive models to a hypersonic flow field ($M = 11$), with $T_s = 294^{o}K$. Other work, Christensen and Buhler (Ref. 2) for example, is not really applicable here since their work is concerned with sublimation rather than liquid ablation.

The experiments presented in this report deals with liquid ablation for two basic cases, i.e. when melting only occurs at the forward point of the model and when melting also occurs along the sides of the model.

4.5.1. Melting with $(T_w)_o \simeq T_m$

In cases where the wall temperature $(T_w)_o$ at the stagnation point was estimated to be in the region of the melting temperature T_m of the model, melting occurred only at the front of the body. For these conditions the recovery temperature along the sides of the model does not reach the melting temperature and thus melting is localised to the stagnation point. As a first approximation it may be expected that the stable shape during melting would be a flat surface normal to the stream direction over which a fairly constant rate of heat transfer exists. This shape was realised in practice (for those temperatures which permitted the recovery temperature along the sides to remain below T_m), see Figs. 14, 15 for example, and could be consistently repeated.

The results from the cine-films of the melting tests are presented in Table 1, where the decrease in length has been tabulated against time. Owing to the natural tendency for T_s to increase with running time it will be observed in some cases that the rate of melting increases after some time has elapsed. Recourse to the filmed records showed that the stable melting shape associated with $(T_w)_o \simeq T_m$ was destroyed when $(T_w)_o$ was considerably greater than T_m, and therefore when mean melting rates were being computed the time interval used was that over which $(T_w)_o \simeq T_m$ existed.

Assuming that the heat transferred to the melting body, under steady conditions, was totally absorbed by the latent heat of fusion some approximate heat transfer rates may be evaluated (Appendix A). Physically these correspond to the rate of heat transfer into a disc of radius equal to the initial nose radius of the hemisphere and are plotted against the radius of the flat nose in Fig. 11. Theoretical estimates of the heat transfer rates were obtained by considering the ideal model of a supersonic airstream impinging on a flat disc (Appendix A), in accordance with the observed stable shapes. This theoretical curve was found to show some agreement with experiment (Fig. 11). Further analysis (Appendix B) allowed the $(x \sim t)$ time histories to be calculated and although agreement with experiment was limited the rate of recession $\frac{dx}{dt}$ was in good agreement, as could be expected (Figs. 12, 13).

4.5.2. Melting with $(T_w)_o$ greater than T_m

For this condition the characteristic truncated cone or hemisphere was no longer obtained and the steady ablating shape was paraboloidal* in nature, the precise shape being temperature dependent for a given Mach number. This was expected, for with the higher stagnation temperatures the recovery temperature along th sides of the model increased and thus the melting was no longer confined to the stagnation point.

When an approximately steady shape at melting was achieved it was found that the rate of recession of the stagnation point was once again constant. With the heat transfer rate based on the total surface area exposed to the heat input, some average values of $\bar{\dot{q}}_i$ consistent in evaluation to those of section 4.5.1 have been obtained. Although the data for $(T_w)_o > T_m$ were limited, the films suggested that for a given value of $(T_w)_o - T_m$ approximately the same shaped paraboloid tended to result and was independent of the initial configuration. This was borne out by the reasonably constant values of $\bar{\dot{q}}_i$ which resulted. That is, for $T_s \sim 512^oK$ the heat transfer rate was estimated to be in the range $4.32 < \bar{\dot{q}}_i < 4.56$ C.H.U./ft^2.sec. for the various initial configurations. These compared with a theoretical value of $\dot{q}_w \simeq 2.71$ C.H.U./ft^2.sec. obtained by considering a turbulent boundary layer to exist over an equivalent shape of paraboloid.

4.6. The Two Dimensional Model

In the design of the wedge model it was necessary to have sufficient thickness to give mechanical strength and to achieve this without choking the tunnel, an asymmetrical wedge was used. This comprised a lower half non-melting wedge of 12° angle on which was superimposed a 6° wedge of the tin-lead eutectic alloy (Fig. 1).

The wedge was tested under stagnation point melting conditions at a Mach number of 1.78. Initial ablation occurred evenly on the middle section of the leading edge and film records (Fig. 20), show the complete sequence. The ablating edge remained approximately parallel to the leading edge for 50 seconds after ablation commenced and was bounded by the convergent lines emanating hear the tips of the leading edge. These bounding lines were at approximately 10° to the stream flow and thus cannot be due to the influence of Mach lines or reflected shock waves discussed previously. As the wedge is effectively at 3° incidence

* A recent paper by L. Lees predicts this phenomena (Ref. 8).

interaction of the leading edge with the tunnel boundary layer this generates a vortex. The area of contact is clearly defined, see Fig. 20, and in the centre of the wedge the model of ablation is in close agreement with the temperature contours of Fig. 9.

Quantitatively, only the rate at which the contour of ablation recedes can be noted from this test. Further tests in which the transient interfacial temperatures are being recorded during ablation are in progress.

5. Conclusions

In these experiments concerned with low melting point materials it was found that the correct choice of model material was an essential requirement if consistent data was to be realised. Of the materials examined the tin-lead eutectic alloy was the only one found to exhibit uniform melting properties and have sufficient mechanical strength at the elevated temperatures to withstand the imposed aerodynamic forces.

The mode of ablation was found to be dependent on the stagnation temperature. When the surface temperature of the model $(T_w)_o$ was approximately equal to the melting temperature T_m the stable shape during melting was a plane normal to the stream direction. For $(T_w)_o > T_m$ the stable shape was of a paraboloidal nature.

For $(T_w)_o \simeq T_m$ the rates of heat transfer, evaluated by considering the heat influx to the model to be completely absorbed by the latent heat of fusion, were found to decrease with increase of the radius of the flat ablating surface. Some agreement with an approximate theory was found.

For $(T_w)_o > T_m$ it was found that the rate of recession of the stagnation point usually reached a constant value and the shape of melting was then steady. Under these steady conditions heat transfer rates were evaluated.

These tests are of a preliminary nature and thus to obtain further insight of the melting process more controlled experiments at higher stagnations temperatures are envisaged.

6. Acknowledgements

The authors wish to acknowledge the generous assistance rendered to them by the staff of the College of Aeronautics, and to express their appreciation of the supervision given by Mr. G. M. Lilley and Mr. J. Busing throughout the period of this work.

7. References

1.	Bogdonoff, S.M.	Exploratory studies of hypersonic fluid mechanics. A.G.A.R.D. Report 142
2.	Christensen, D., Buhler, R.D.	On the stable shape of an ablating graphite body. J. Aero. Space Scs. Vol.26 No. 1
3.	Fordham, L.H.	Report on the propulsion department's supersonic wind tunnel. Thesis 10/22 C. of A. June 1957
4.	Homer, C.E., Plummer, H.	Embrittlement of tin at elevated temperature and its relationship to impurities. J. Inst. Met. Vol. LXIV, 1939.
5.	Roberts, L.	Stagnation point shielding by melting and vaporisation. N.A.S.A. Report 10.
6.	Seel, M.W.R.	The design and assessment of a supersonic hot air tunnel and associated equipment for conducting heat transfer and drag measurements on melting bodies. Thesis E11/5 C. of A. June 1958.
7.	Seel, M.W.R.	Preliminary report on melting bodies. Unpublished Laboratory C.of.A. Report, Aug. 1958.
8.	Lees, L.	Ablation in hypersonic flows. I.A.S. Paper No. 59 - 146 1959.

APPENDIX A

Simplified Analysis of Melting for which $(T_w)_o \simeq T_m$

For the purpose of this analysis it is assumed that the temperature inside the model and the temperature at the gas-liquid interface are approximately equal to the melting temperature of the model T_m. Under such conditions the rate of heat transfer per unit area $\dot{q}_i$, into the body is roughly that absorbed by the latent heat of melting L_m, and is

$$\dot{q}_i \simeq \frac{L_m \dot{m}}{A} \qquad \text{A1.}$$

$\dot{m}$ is the rate at which material is lost and A is the area over which heat is being transferred. It will be noted that the above equation makes no allowance for the heat absorbed by the body, the heat absorbed by the liquid layer, and the rate at which heat is convected away from the stagnation point by the liquid layer.

The local heat transfer rate at the stagnation point of a non-ablating body may be expressed in terms of the Nusselt No. (Nu) and the local Reynolds No. (Re) as

$$(\dot{q}_w) = \frac{C_{p_w}(T_e - T_m)}{\sigma} \sqrt{\rho_w \mu_w \frac{dU_e}{dr}} \cdot \frac{Nu}{\sqrt{Re}} \qquad \text{A2.}$$

where

C_{p_w} = specific heat of the gas at the wall

T_e = temperature just outside the boundary layer

T_m = melting temperature of the model = $(T_w)_o$ the wall temperature

ρ_w = density at the wall

μ_w = viscosity at the wall

$\frac{dU_e}{dr}$ = velocity gradient

r = distance measured from the stagnation point along the body surface

Nu = Nusselt No. = $r\left(\frac{\partial T}{\partial y}\right)_w / (T_e - T_m)$

Re = Reynolds No. = $\rho_w U_e r / \mu_w$

σ = Prandtl No. at the wall

For the cases in which $(T_w)_o \simeq T_m$ experiment suggested that for all configurations the resulting stable shape of melting was a flat plane perpendicular to the free stream. Thus when approximating the value of $\frac{dU_e}{dr}$ in equation 2 an ideal model of a supersonic gas-stream impinging on a flat disc was considered. By considering the subsonic flow of an inviscid liquid over a circular disc potential theory yields

$$\frac{dU_e}{dr} = \frac{2}{\pi} \cdot \frac{U_s}{R} \left[1 - \frac{r^2}{R^2} \right]^{-3/2}$$

where U_s is the velocity just behind the detached shock wave and R is the radius of the disc. This together with the assumption that $Nu/\sqrt{Re} = 0.806\ \sigma^{0.4}$ gives

$$(\dot{q}_w) \simeq \left\{ \rho_w U_s C_{p_w} (T_e - T_m) \sqrt{\frac{2\mu_w}{\pi \rho_w U_s R}}\ 0.806\ \sigma^{0.6} \right\} \left(1 - \frac{r^2}{R^2} \right)^{-\frac{3}{4}} \qquad A3$$

as the local heat transfer rate over the disc.
The total heat input per unit time over the whole disc is

$$(\dot{Q}) = 4\pi R^2 D$$

where D is the expression in the curly brackets of equation A3.

Defining $(\bar{\dot{q}}_w) = \frac{1}{2} \frac{\dot{Q}}{\pi R^2}$ to be an average value of the rate of heat transfer over the whole disc then

$$(\bar{\dot{q}}_w) \simeq 2 \rho_w U_s C_{p_w} (T_e - T_m) \sqrt{\frac{2\mu_w}{\pi \rho_w U_s R}}\ 0.806\ \sigma^{-0.6} \qquad A4$$

Taking $\rho_w \simeq \rho_s$, $\mu_w \simeq \mu_s \simeq \mu_\infty$ where the subscripts 's' and '∞' denote conditions just behind the detached shock and free stream conditions, and noting that $\rho_s U_s = \rho_\infty U_\infty$ under ideal normal shock conditions, then equation A4 may be written in the more convenient form of

$$(\bar{\dot{q}}_w) = \left\{ \frac{M_\infty \rho_o a_o}{\left(1 + \frac{\gamma - 1}{2} M_\infty^2 \right)^{\frac{\gamma+1}{2(\gamma-1)}}} \right\} \sqrt{\frac{C_{p_w} (T_e - T_m)}{\frac{\pi}{8} \frac{\rho_\infty U_\infty}{\mu_\infty} R}}\ 0.806\ \sigma^{-0.6} \qquad A5$$

Here ρ_o, a_o denote the stagnation values of the density and speed of sound, and for numerical results it is assumed that T_e realises the stagnation value.

APPENDIX B

Ablation of cones and hemispheres for which $(T_w)_o \simeq T_m$

For fixed conditions, i.e. known constant values of M_∞, ρ_o, a_o, C_{p_w}, $(T_e - T_m)$ etc., equation A5 may be written

$$(\bar{q}_w) = \frac{C}{\sqrt{R}} \qquad \text{B1}$$

where C is a constant for the prescribed conditions. For a Truncated Cone it is readily seen that equation A1 becomes

$$\bar{q}_i = \frac{L_m \rho_m}{A} \left(\pi^2 x^2 \tan^2 \frac{\theta}{2} \right) \frac{dx}{dt} \qquad \text{B2}$$

for a particular value of the cone angle θ, x is the distance which the stagnation point of the melting cone has recessed. With the heat transfer rate based on the area of the flat ablating disc, i.e.

$A = \pi^2 x^2 \tan^2 \theta/2$, then

$$\bar{q}_i = L_m \rho_m \frac{dx}{dt} \qquad \text{B3}$$

gives an experimental estimate of rate of heat transfer into a disc of area $\pi^2 x^2 \tan^2 \frac{\theta}{2}$, provided $\frac{dx}{dt}$ is known. Experiment has shown (Fig. 12), that equation B1 provides a good estimation of the heat transfer rates, therefore assuming the liquid layer is thin, then equating B1 and B3 gives

$$\frac{dx}{dt} = \frac{C}{L_m \rho_m} \sqrt{R}$$

From Fig. 10b it is seen that

$$\frac{dx}{dt} = \frac{C}{L_m \rho_m} \frac{1}{\sqrt{x \tan \frac{\theta}{2}}} \qquad \text{B4}$$

Integration of B4 gives the time history of the recession of the stagnation point, that is

$$x^{\frac{3}{2}} = \frac{3}{2} \frac{C}{L_m \rho_m} \frac{t}{\sqrt{\tan \frac{\theta}{2}}} \qquad \text{B5}$$

This has been compared with experiment in Fig. 13.

TABLES OF RESULTS FOR MELTING TESTS

15° Cone
Zero Nose Radius
$T_s \simeq 485°K$

t(secs)	x
0	0
2.7	0.23
6.0	0.44
7.8	0.48
9.2	0.57
10.8	0.64
12.3	0.72
13.8	0.74
15.4	0.77
17.0	0.79
18.5	0.81
21.7	0.88
24.8	0.93
28.0	0.98
31.0	10.40
34.5	10.80

15° Cone
1/16" Nose Radius
$T_s \simeq 485°K$

t	x
0	0
9.7	0.05
15.7	0.06
22.0	0.10
28.2	0.16
34.5	0.19
40.0	0.24

15° Cone
3/16" Nose Radius
$T_s \simeq 482°K$

t	x
0	0
1.0	0.02
4.1	0.03
7.4	0.07
10.5	0.10
12.4	0.11
16.6	0.16
19.8	0.20
22.8	0.21
26.1	0.23
29.2	0.25
32.2	0.30

20° Cone
3/16" Nose Radius
$T_s \simeq 482°K$

t	x
0	0
3.8	0.02
14.0	0.035
47.0	0.080
65.5	0.120
78.0	0.165

20° Cone
5/16" Nose Radius
$T_s \simeq 491°K$

t	x
0	0
5.8	0.03
23.6	0.045
34.8	0.08
47.5	0.12

25° Cone
Zero Nose Radius
$T_s \simeq 483°K$

t	x
0	0
1.5	0.05
2.7	0.09
4.1	0.12
5.1	0.13
7.6	0.19
8.9	0.24
10.25	0.28
11.40	0.29
12.70	0.33
13.80	0.35
16.40	0.40
20.30	0.43
24.0	0.52
27.6	0.55
31.5	0.59
37.7	0.71

25° Cone
3/16" Nose Radius
$T_s \simeq 512°K$

t	x
0	0
4.0	0.10
8.1	0.18
13.0	0.26
18.1	0.40
21.8	0.50

A similar analysis for hemispherical models (Fig. 10c), shows that the time history of recession of the stagnation point is

$$t = \frac{R^{\frac{3}{2}} L_m \rho_m}{C} \int_0^{x/R} \left\{ 1 - (p-1)^2 \right\}^{\frac{1}{4}} dp \,, \qquad \text{B6}$$

which has been integrated numerically and compared with the experimental values, (Fig. 14). Once again it should be noted that $\dot{q}_i$ is based on the area of the flat ablating disc.

25° Cone
Zero Nose Radius
$T_s \simeq 491°K$

t	x
0	0
2.1	0.07
3.4	0.11
5.0	0.15
7.0	0.21
8.2	0.29
10.0	0.37
11.5	0.40
12.9	0.47
14.5	0.53
16.0	0.54
17.6	0.58
20.8	0.68
23.8	0.74
27.0	0.79
34.5	1.05

25° Cone
5/16" Nose Radius
$T_s \simeq 512°K$

t	x
0	0
4.3	0.05
7.0	0.10
11.5	0.17
15.0	0.34
19.3	0.45
21.75	0.56

25° Cone
Zero Nose Radius
$T_s \simeq 512°K$

t	x
0	0
2.5	0.13
3.9	0.23
5.0	0.25
6.1	0.30
8.3	0.34
9.0	0.35
10.0	0.41
11.3	0.48
12.5	0.50
15.0	0.57
17.6	0.67
22.5	0.86
25.0	1.0
27.6	1.18

25° Cone
1/16" Nose Radius
$T_s \simeq 522°K$

t	x
0	0
1.6	0.09
3.7	0.20
6.4	0.34
9.7	0.46
12.3	0.63
15.4	0.80
16.7	0.90

25° Cone
Zero Nose Radius
$T_s \simeq 522°K$

t	x
0	0
3.5	0.23
5.8	0.36
14.5	0.95
18.3	1.13
21.5	1.38

30° Cone
Zero Nose Radius
$T_s \simeq 489°K$

t	x
0	0
6.1	0.06
7.8	0.11
11.6	0.15
20.0	0.29
24.0	0.35
29.0	0.44
34.5	0.51
38.6	0.59
44.0	0.67
49.5	0.78
58.5	0.93
67.0	1.08

30° Cone
$\frac{1}{8}$" Nose Radius
$T_s \simeq 484°K$

t	x
0	0
13.6	0.05
19.5	0.10
27.0	0.23
33.0	0.29
40.8	0.39
49.4	0.51
60.0	0.65

30° Cone
$\frac{1}{4}$" Nose Radius
$T_s \simeq 490°K$

t	x
0	0
7.0	0.03
26.0	0.07
38.0	0.11
47.5	0.17
55.4	0.24
63.5	0.33
73.0	0.40

35° Cone
Zero Nose Radius
$T_s \simeq 486°K$

t	x
0	0
1.8	0.07
3.5	0.15
5.2	0.20
7.0	0.25
8.5	0.31
10.3	0.34
11.7	0.36
13.1	0.39
14.7	0.40
16.3	0.42
17.9	0.43
20.4	0.46
24.3	0.48
27.0	0.52
30.4	0.56

35° Cone
3/16" Nose Radius
$T_s \simeq 485°K$

t	x
0	0
4.1	0.04
11.8	0.10
20.4	0.17
28.4	0.25
33.7	0.35

30° Cone
3/16" Nose Radius
$T_s \simeq 489°K$

t	x
0	0
8.4	0.04
17.5	0.07
27.0	0.12
35.0	0.19
45.0	0.29
54.3	0.40
65.0	0.48
75.5	0.60

35° Cone
Zero Nose Radius
$T_s \simeq 535°K$

t	x
0	0
9.2	0.32
14.1	0.47
18.7	0.77

40° Cone
Zero Nose Radius
$T_s \simeq 489°K$

t	x
0	0
2.8	0.05
5.5	0.08
8.5	0.14
12.6	0.19
16.5	0.27
21.0	0.34
26.8	0.41
32.2	0.52
37.1	0.59

40° Cone
1/16" Nose Radius
$T_s \simeq 480°K$

t	x
0	0
18	0.16
24	0.20
33	0.29
46	0.38
54.5	0.44
68.8	0.54

40° Cone
3/16" Nose Radius
$T_s \simeq 484°K$

t	x
0	0
8.6	0.04
15.8	0.08
25.5	0.16
36.7	0.23
45.4	0.33
56.1	0.41
64.0	0.50

40° Cone
3/16" Nose Radius
$T_s \simeq 488°K$

t	x
0	0
19.4	0.07
32.2	0.11
43.2	0.17
55.0	0.20
66.7	0.25
78.5	0.31

Wedge Model

$T_s \simeq 485°K$

t	x
0	0
5.5	0.04
17.4	0.13
25.0	0.29
34.0	0.38
48.0	0.47
55.0	0.57
66.0	0.63
74.0	0.75

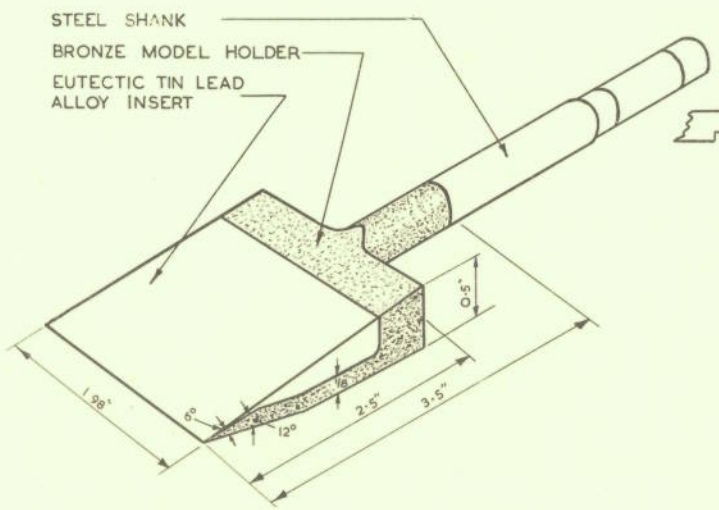

FIG. 1. WEDGE MODEL

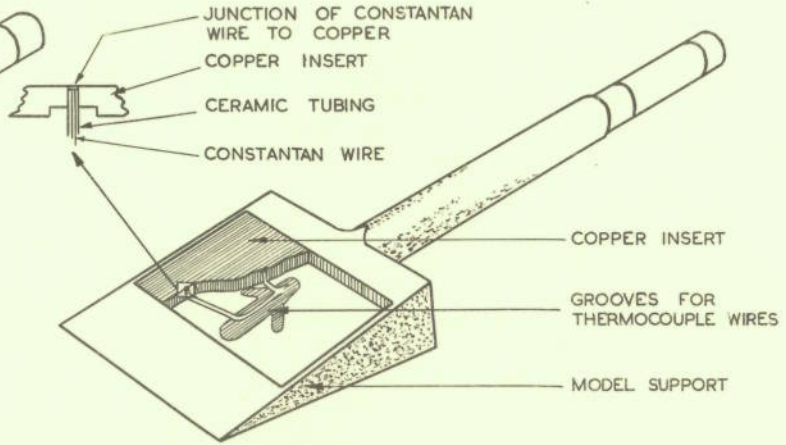

FIG. 2. WEDGE MODEL FOR MEASURMENT OF SURFACE TEMPERATURE

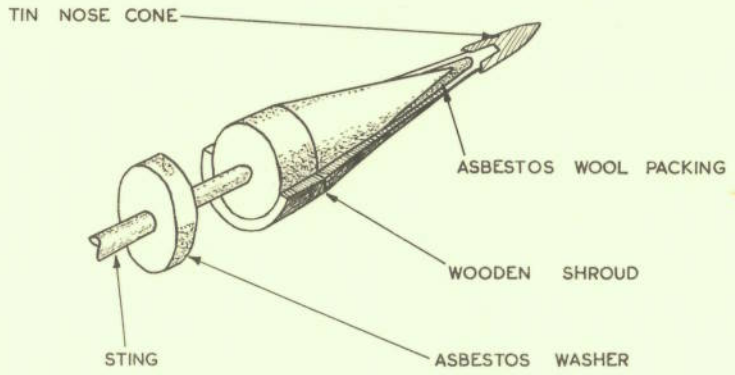

FIG. 3. THE SHROUD MODEL

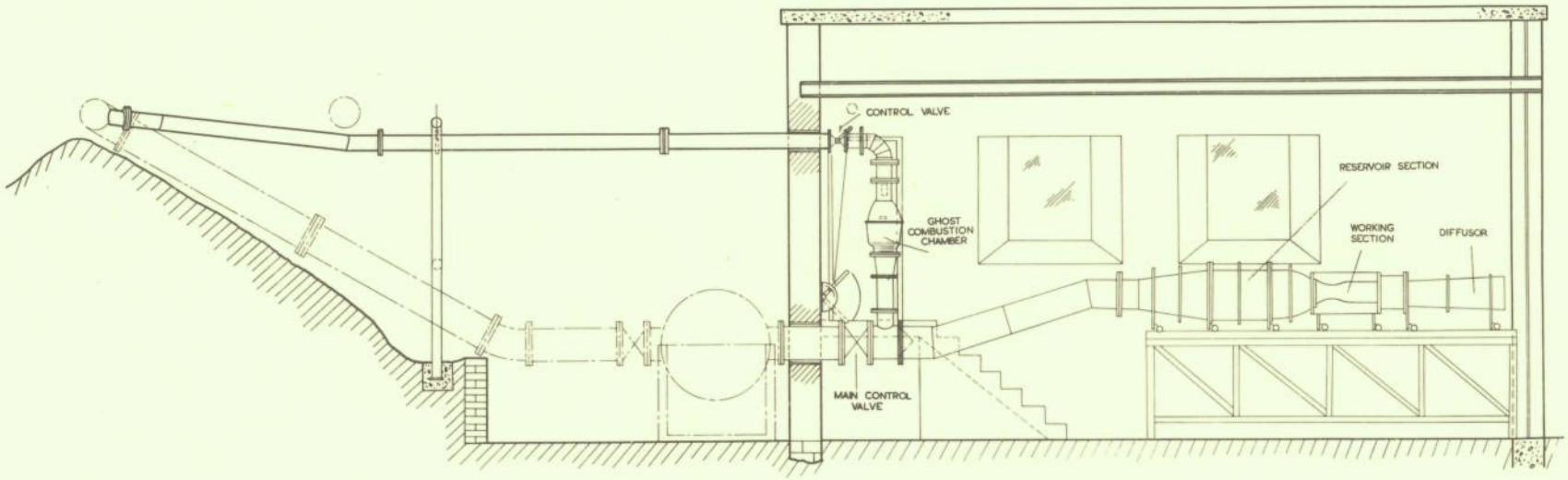

FIG. 4. GENERAL LAYOUT OF TUNNEL

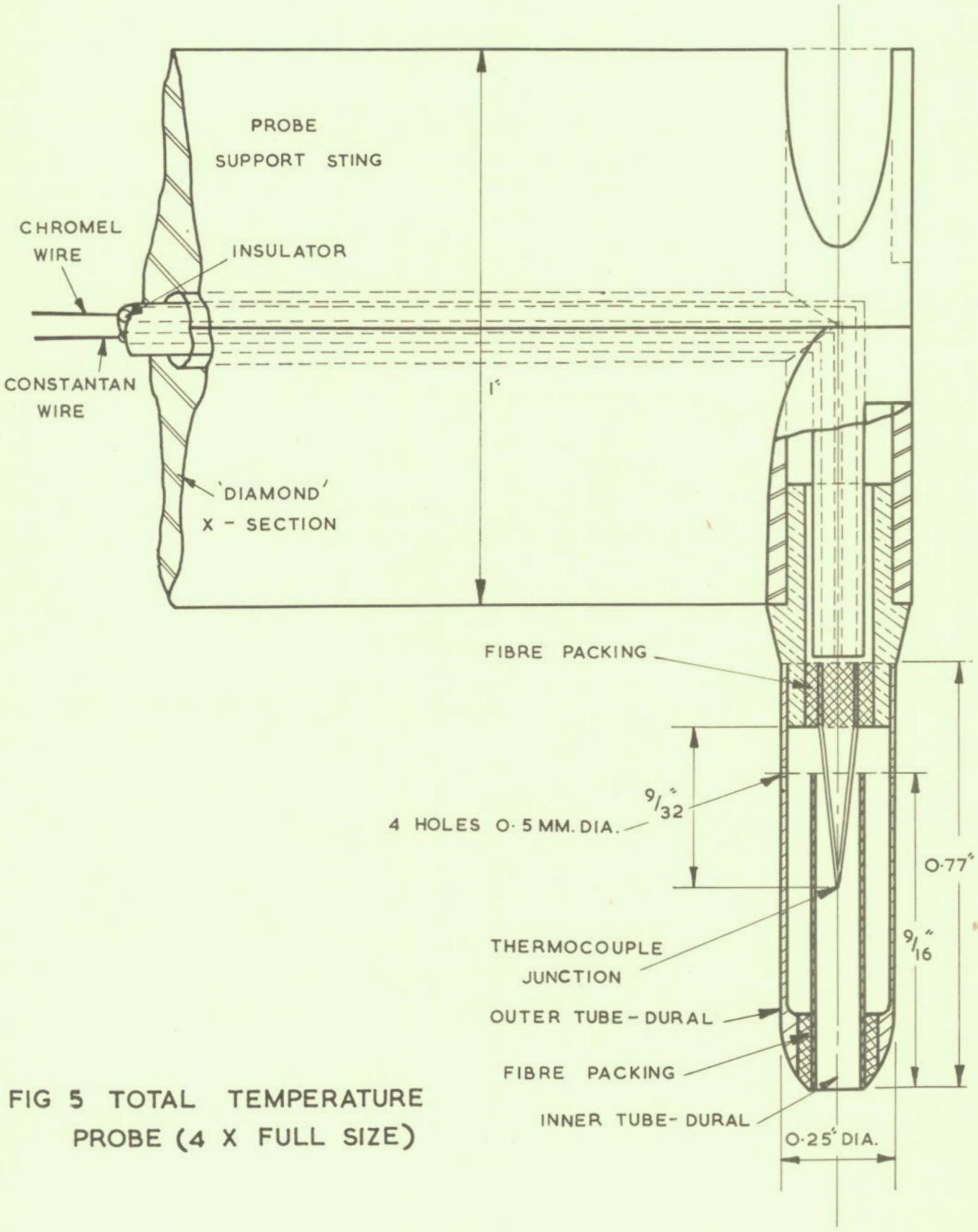

FIG 5 TOTAL TEMPERATURE PROBE (4 X FULL SIZE)

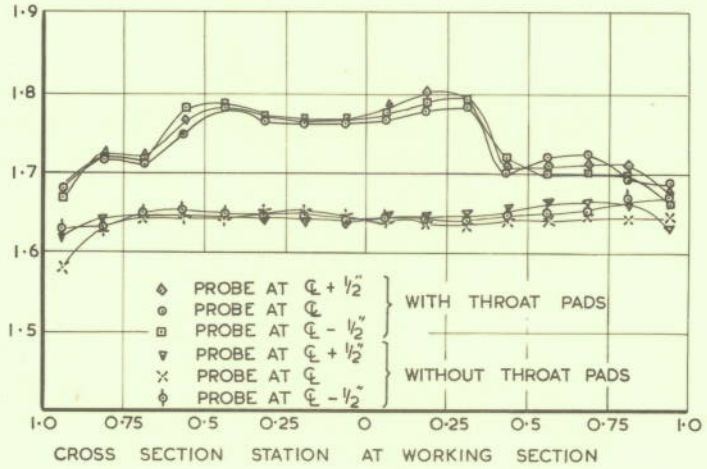

FIG. 6. MACH NUMBER VARIATION AT WORKING SECTION

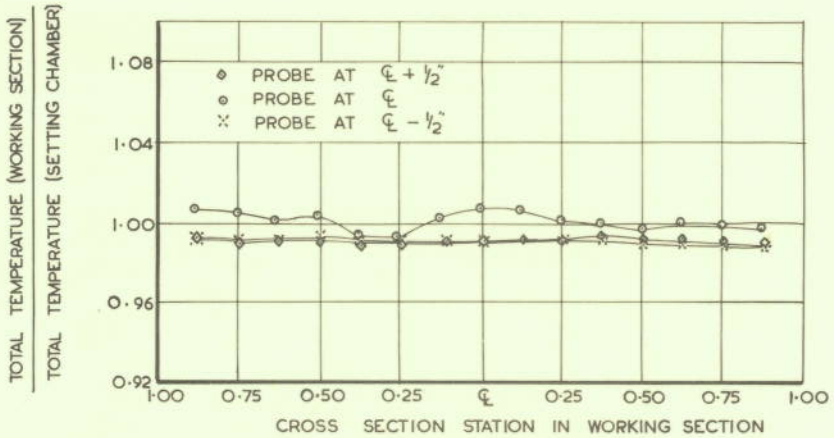

FIG. 7. VARIATION TOTAL TEMPERATURE AT WORKING SECTION

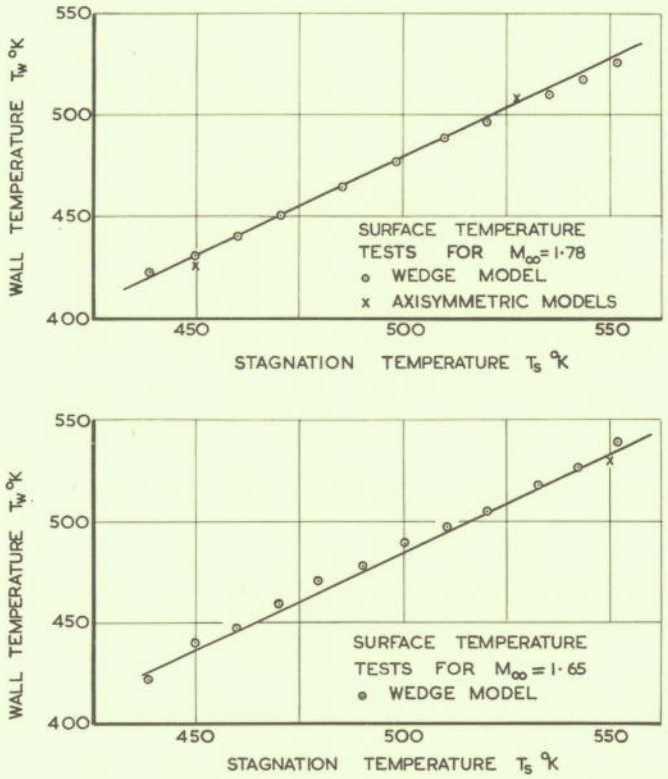

FIG. 8. VARIATION OF WALL TEMPERATURE ON WEDGE MODEL WITH STAGNATION TEMPERATURE

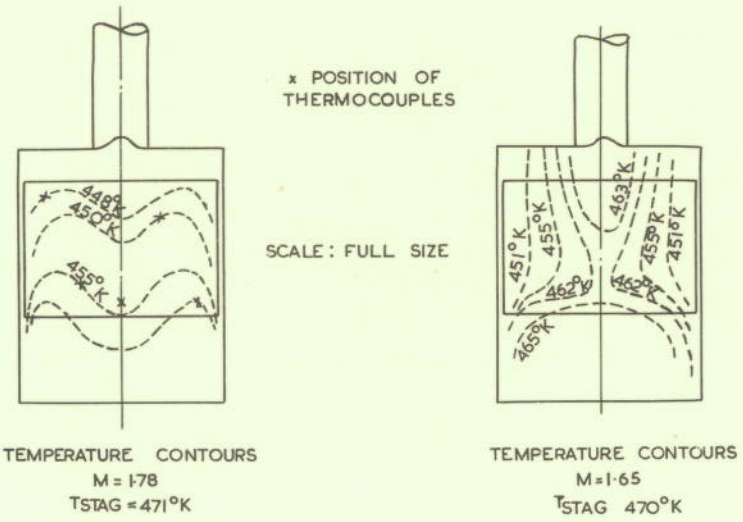

FIG. 9.

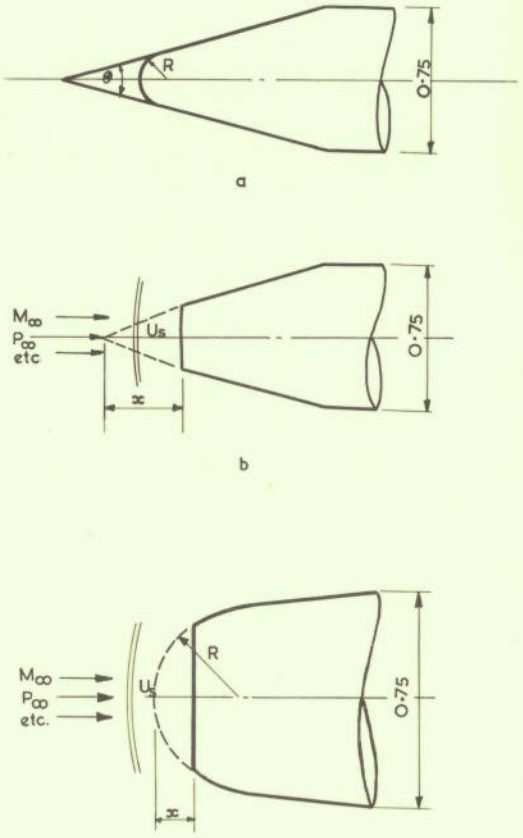

FIG. 10. IDEAL MODELS USED IN APPENDIX A

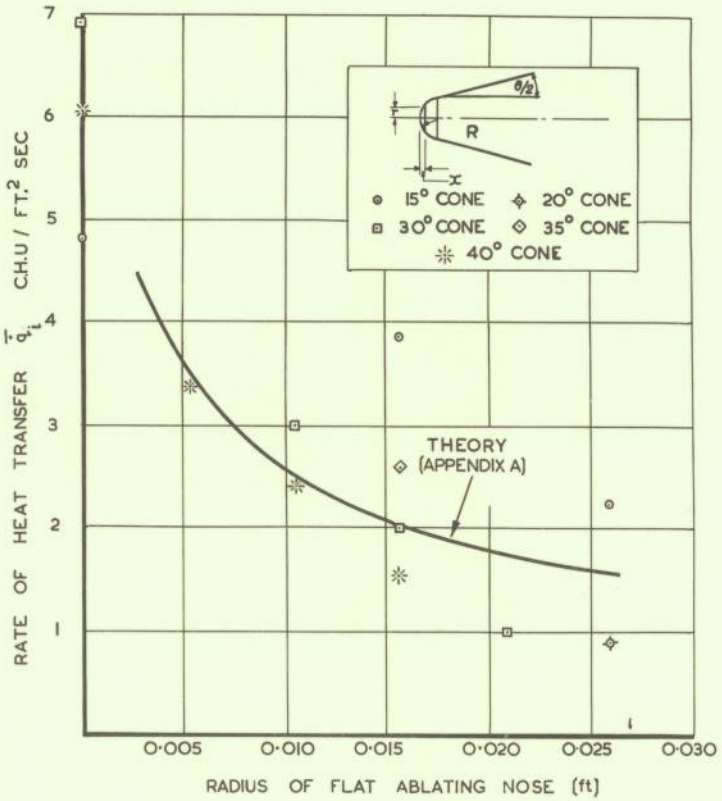

FIG. 11. RATE OF HEAT TRANSFER - NOSE RADIUS FOR $M = 1{\cdot}78$ AND $(T_W)_o \simeq T_m$

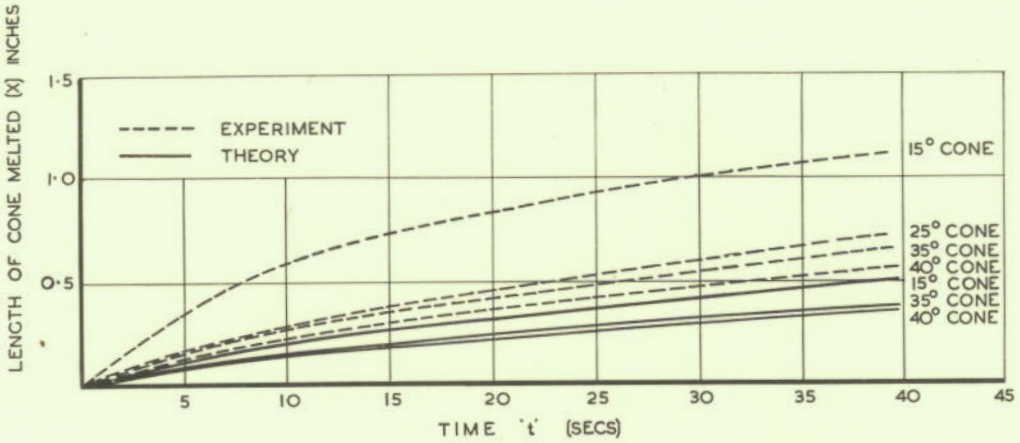

FIG. 12. COMPARISON OF THEORY WITH EXPERIMENT FOR THE TRANSIENT MELTING OF A CONE AT M=1·78 AND $(T_w)_o \simeq T_m$

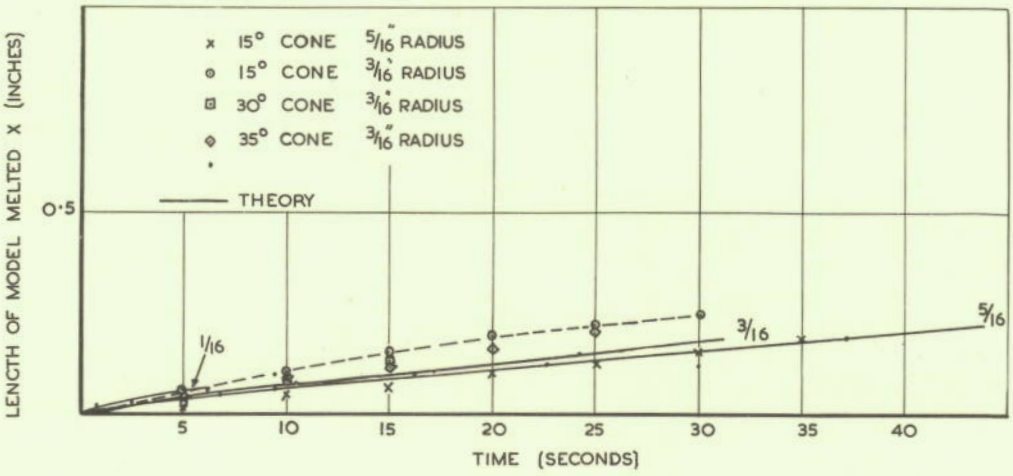

FIG. 13. COMPARISON OF THEORY WITH EXPERIMENT FOR THE TRANSIENT MELTING OF HEMISPHERE CONE MODELS AT M=1·78 AND $(T_w)_o \simeq T_m$

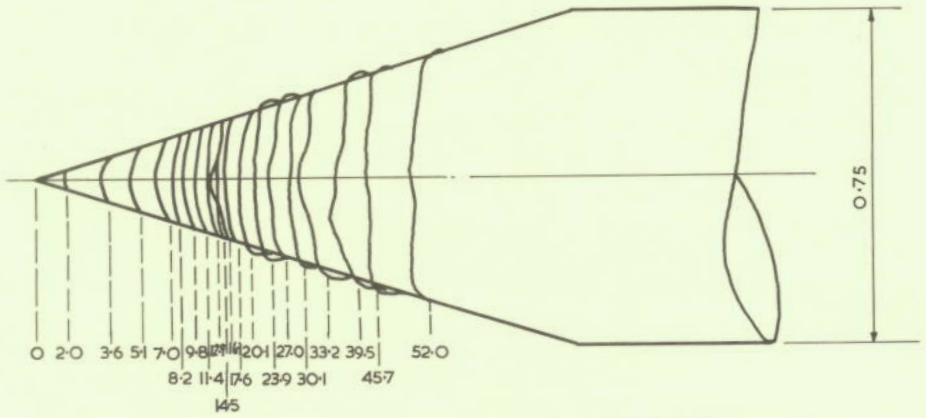

CONE ANGLE: 35°
MATERIAL: Sn 63% Pb 37%
STAGNATION TEMP. 484°K
MACH NO. 1·78

FIG. 14.

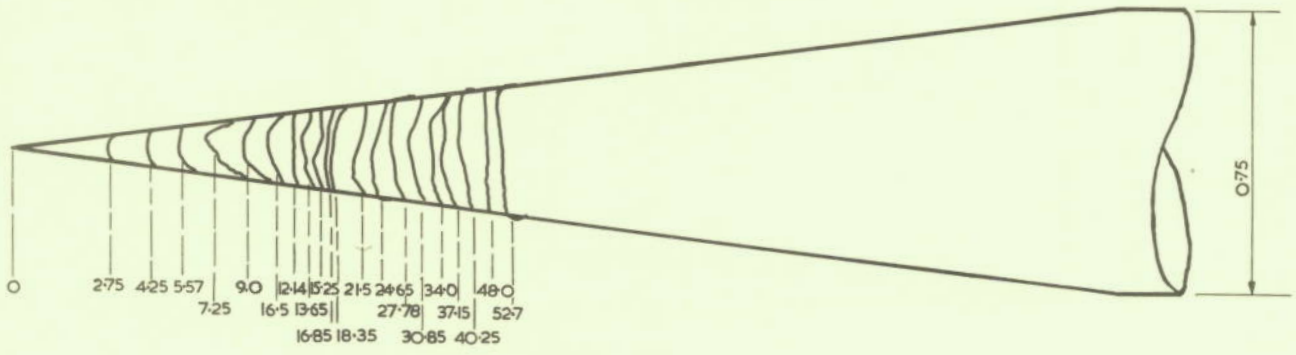

CONE ANGLE: 15°
MATERIAL: EUTECTIC ALLOY Su 63% Pb 37%
STAGNATION TEMP 485°K
MACH NO 1·78

FIG. 15

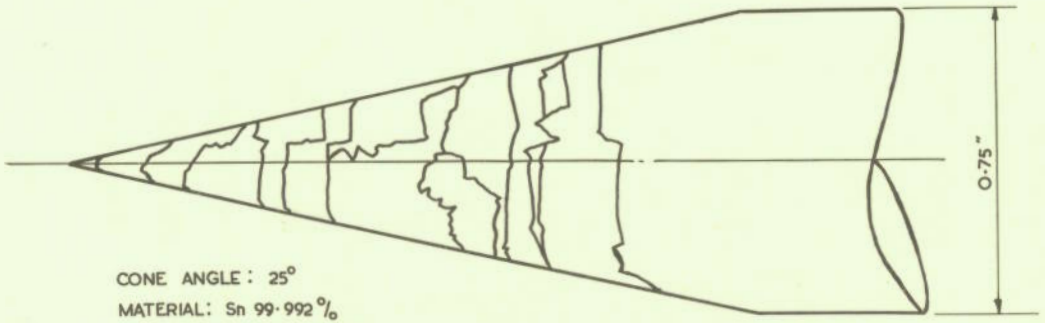

CONE ANGLE : 25°
MATERIAL: Sn 99·992 %
STAGNATION TEMP. 528° K
MACH NO 1·78

FIG. 16.

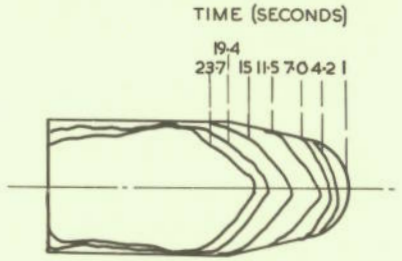

CONE ANGLE: 25°
NOSE RADIUS: 5/16"
MATERIAL Sn 63% Pb 37%
STAGNATION TEMP 512°K
MACH NO 1·78

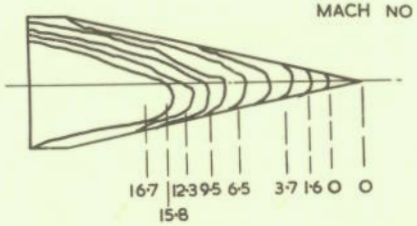

CONE ANGLE: 25°
NOSE RADIUS: 2/16"
MATERIAL Sn 63% Pb 37%
STAGNATION TEMP 522°K
MACH NO. 1·78

FIG. 17.

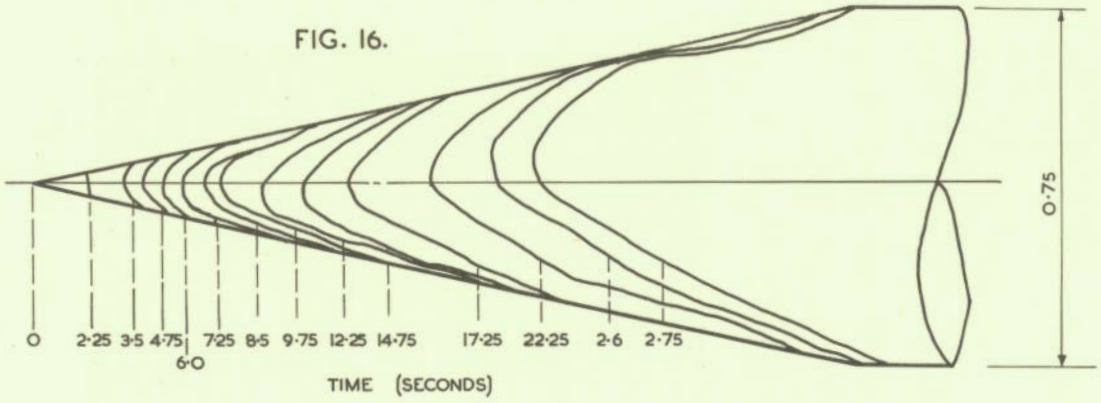

CONE ANGLE: 25°
MATERIAL: Sn 63% Pb 37%
STAGNATION TEMP. 512° K
MACH NO. 1·78

FIG. 18.

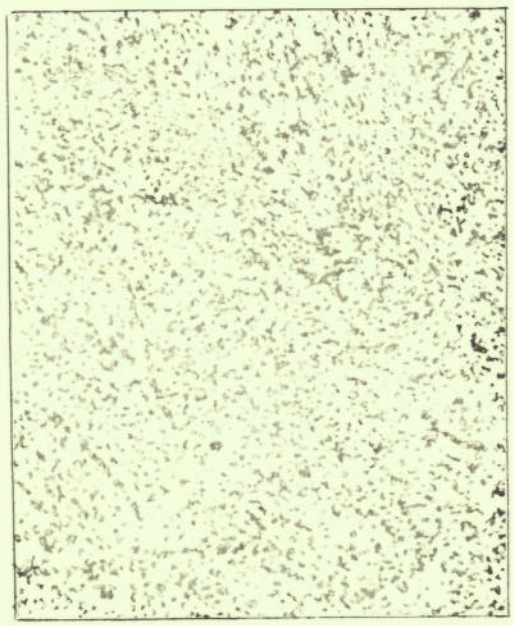

a. EUTECTIC TIN-LEAD ALLOY
Pb 37% Sn 63%
MAG. x 450

b. CHEMPUR TIN
Sn 99·992%
MAG × 500

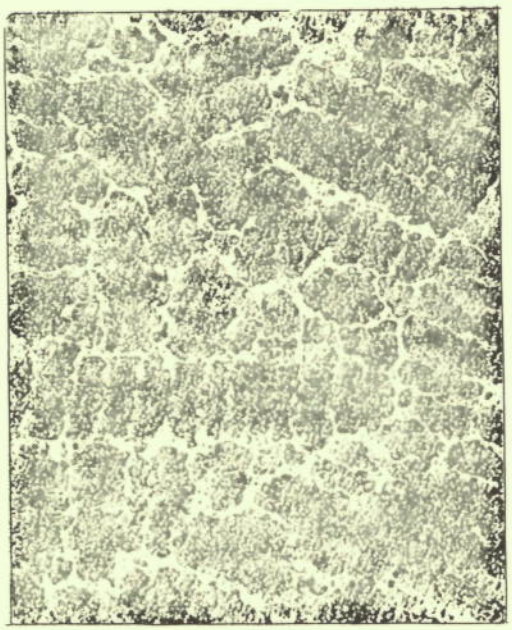

c. TIN LEAD ALLOY
Pb 60% Sn 40%
MAG.x 140

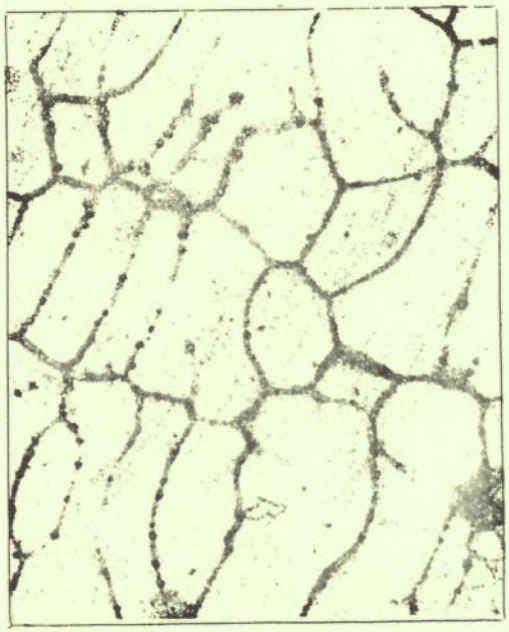

d Nº2 COMMERCIAL TIN
Sn 99.992%
MAG.x 140

FIG. 19 PHOTO MICROGRAPHS

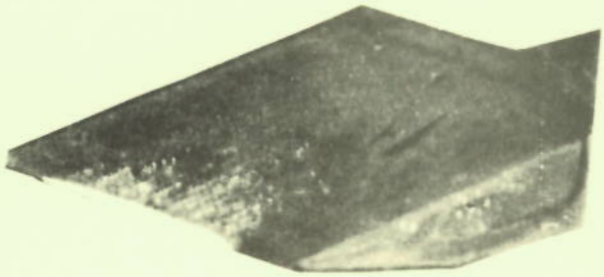

t = 2·5 secs

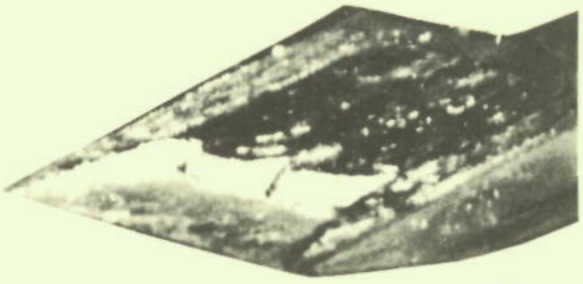

t = 81·6 secs

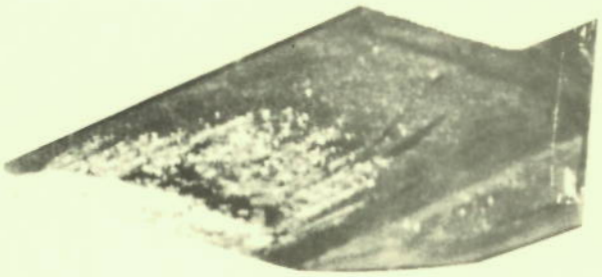

t = 21·4 secs

t = 111 secs

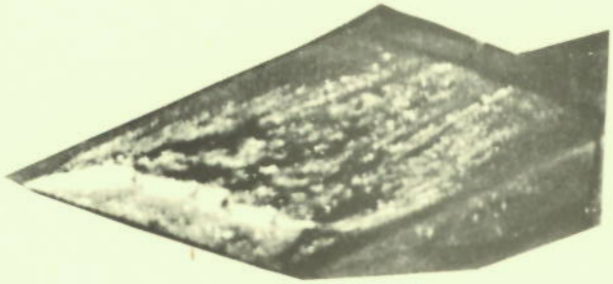

t = 40·2 secs

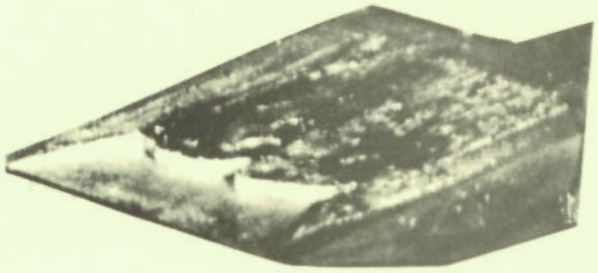

t = 60·5 secs

FIG. 20 WEDGE MODEL

TSTAG = 485° K